

Chapter 4

Comparison of FENE and FJC molecules

4.1 Introduction

We have seen in the previous chapter (Section 3.3.1) that there are many molecular potentials available for simulating polymeric liquids. Despite the large collection of potentials available, we have also acknowledged in Chapter 2 that many of the properties of polymeric liquids are independent of the specific molecule being investigated. In this chapter we compare some of the rheological and structural properties of two molecules which we name the *finitely extensible nonlinear elastic* molecule (FENE) and the *freely jointed chain* molecule (FJC).

We present and discuss the results from NEMD simulations of the FJC molecules and FENE molecules. The basis of comparison will be the commonly calculated steady state rheological properties, such as viscosities and normal stresses, along with some structural properties which can be readily calculated in molecular simulations. The previous chapter has already presented the simulation algorithms and techniques that we use, this chapter includes some computational detail, a summary of the length of simulations

etc., along with necessary details of how averages were calculated. From the outset there were several reasons for making the comparison between the FENE and FJC molecules. The first was to investigate the effect that the flexibility of the bond length of the FENE molecules had on the macroscopic properties. Secondly, the force calculation for the FENE molecules was less involved than the method used to calculate constraint forces of the FJC molecules and so it was interesting to compare the computational efficiency of the two models. Thirdly, the data presented in this chapter are rheological and structural and provide a useful background for the next chapter: Chapter 5 on the self-diffusion of molecules in shear and extensional flows.

In the next section (4.2) we review the previous works in the literature which we feel are relevant to the investigation here. In Section 4.3 we look at the simulation details. This is followed in Section 4.4 by analysis of the average bond length in the FENE systems and a choice of the bond length for the FJC systems is made. Section 4.5 presents the results from the simulations we have performed, which include viscoelastic, dynamic and structural properties. Some of these properties are compared qualitatively with predictions of the Curtiss-Bird and Doi-Edwards models from Chapter 2.

4.2 Review

4.2.1 The FJC molecule

In the work of Evans *et al.* [EHF⁺83] the connection had been made between algorithms for nonequilibrium systems at constant temperature and Gauss' principle of least constraint. Subsequently this principle was used to simulate molecules with constrained bond length and bond angles [EEM86, ME91] and has been used for the simulation of both linear and branched molecules. The studies that we are interested in here are the simulations of linear

molecules. This includes the work of Matin *et al.* [MDT00, MDT03], the thesis of Matin [Mat01] and works by Daivis *et al.* [DMT03, DMT07]. We also note that the model has been used to simulate linear molecules in solution [KDMS04a, KDMS04b] as well as polymer melts containing spherical filler particles [KDIB05].

The papers which we review in this section all presented steady state results for both planar Couette flow and planar extensional flow. The paper of Matin *et al.* [MDT00] was the first publication of results using the KR pbc for PEF and the molecular SLLOD algorithm, which we described in the previous chapter. The authors simulated a model of chlorine which had been used in several previous publications [HPR92, TDE95a, TDE95b, EEM87]. This model consisted of Lennard Jones dimers bonded using the Gaussian constraint algorithm. These simulations confirmed that under PEF, molecules have zero average spin angular velocity, a quantity which had been measured under PCF in the previous publications; we discuss this topic further in Section 4.5.2. In addition to the chlorine molecules Matin *et al.* simulated liquids of Lennard Jones atoms as well as two-site and four-site FJC molecules. It was confirmed that the atomic systems had little elasticity since the first normal stress ($N_1 = P_{yy} - P_{xx}$) was found to be approximately zero, except at the highest strain rate. For molecular systems it was found that N_1 deviated significantly from zero as the strain rate increased and was attributed to the elasticity of the molecular fluid [BAH87]. Further results for the two-site FJC molecules were published by Matin *et al.* [MDT03]. In that study it was found that independent calculation for PCF and PEF of the coefficients of the third order retarded motion expansion (RME) led to consistent results. Examination of the conditions for which the ratio $\eta_1/\eta_2 \approx 0$ led the authors to conclude that the Newtonian regime extended to $\dot{\epsilon} = 0.0296$. This was in agreement with their plot of viscosity against strain rate.

Subsequent simulations of longer molecules have been presented in the papers of Daivis, Matin and Todd [DMT03, DMT07] which relied significantly on the results presented in the thesis of Matin [Mat01]. In the first of the papers [DMT03] systems of 4-site up to 50-site molecules were simulated. It was found that lower order coefficients for the RME were in agreement when calculated using data from PCF and PEF. However, it was found that the higher order terms did not have the same level of agreement. This was attributed to large uncertainties in the results for longer molecules at low strain rates. Calculation of the N_s dependence (number of sites per molecule) of η_0 and the zero strain rate first normal stress $\Psi_{1,0}$ agreed with the Rouse model predictions that $\eta_0 \propto N_s$ and $\Psi_{1,0} \propto N_s^3$.

Improvement on these results was presented in the second paper [DMT07]. There, chain lengths of up to $N_s = 100$ were simulated. The agreement between calculated coefficients of the RME was found for terms up to second order in the strain rate. Disagreement was found in the third order terms calculated from the normal stress coefficients of PEF η_1 and η_2 . It was suggested that this discrepancy was due to a mismatch between the assumptions of the RME and the conditions of the simulation.

The code that we have used during this thesis was a version of the code used for the FJC publications cited above. We have then changed the molecular potential to the FENE potential for the comparison of the two models. We have also added subroutines to calculate the diffusion coefficient and the velocity autocorrelation functions that we describe in the next chapter.

4.2.2 The FENE molecule

Several significant studies have used the FENE model to investigate rheological properties of polymer melts. Indeed this was one of our main motivations for comparing the FENE and FJC molecules. Kröger, Loose and Hess [KLH93] investigated rheological and structural properties of a monodisperse

FENE melt under PCF with molecules between $N_s = 10$ to $N_s = 100$ in length. These simulations used the atomic SLLOD algorithm together with the atomic thermostat, and it is not clear whether this algorithm led to over alignment in the system that had been observed in other molecular simulations using this algorithm [TDE95a]. However, the range of data presented in this work is very significant. Two methods were used to calculate the structure of the liquid: firstly the alignment tensor was calculated, and through this the alignment angle of molecules (in Section 4.5.2 we introduce the order tensor which is closely related to the alignment tensor). Secondly, the structure factor was calculated and compared favourably with experimental results from small angle neutron scattering experiments [MPP93]. Comparing the alignment tensor and the stress tensor confirmed the stress-optic law in the Newtonian regime. It was shown that the Rouse prediction for the chain-length dependence of the viscosity $\eta_0 \propto N_s$ was confirmed for chains of length $N_s \leq 60$, with a slight up-turn in this curve for $N_s = 100$, suggesting that the crossover between the Rouse and reptation regime had been reached. This last observation was confirmed by Kröger and Hess [KH00] in a publication which presented steady state viscosities of monodisperse FENE systems ranging in length from $N_s = 10$ up to $N_s = 400$.

In the case of extensional flows, Kröger, Luap and Muller [KLM97] investigated the start-up of UEF and subsequent relaxation. The authors compared experimental observations of molecular alignment and stress measurements with similar measurements from NEMD simulation. These measurements allowed them to determine the range of validity of the stress-optic law, the linear relationship between the stress and alignment of bond vectors in the liquid. In the start-up phase of the simulations and experiments, they found that the stress-optic law was valid at low strain-rates and at high temperatures. However, in the relaxation phase it was found that the rule was valid for all systems. At high strain-rates a stress offset was observed

which was found to have a linear dependence on the strain rate.

Boško *et al.* [BTS04a, BTS04b, Boś05] have performed simulations under PCF of dendrimer liquids, where the molecules were composed of beads connected by the same FENE potential that we have used here. They have compared their results with simulations of linear FENE molecules. In references [BTS04a, BTS04b] the simulations were performed using molecular SLLOD at constant volume. The reduced temperature of these systems was $T = 1.25$ and the density was $\rho = 0.84$, which is different to the state-point used in our work. They investigated viscoelastic and structural properties, most of which we have investigated here for linear molecules (the state point of this system is given in reduced units which we discuss further on page 99). For the properties which are common between this investigation and their investigation we have included a comparison in the relevant sections below. Three properties Boško *et al.* investigated, which we have not included in our investigation, are: the radial distribution between the centre of mass of molecules, radial distribution of the terminal groups of the molecules from the centre of the molecule and the fractal dimension of the molecule.

4.2.3 Studies with varied molecular properties

Several authors have used Brownian dynamics simulations to investigate the effect of molecular properties on the mobility of molecules as well as structural properties of model polymer melts at equilibrium. These authors employed the technique that had been used by Grest and Kremer in their investigations of Rouse and reptative dynamics [GK86, KG90].

Feller *et al.* [Fal00, FMPH00] have used the FENE molecular potential combining it with a three-body torsional potential to determine the effect of chain stiffness and chain length on the reorientation times of chain segments. They found that there were two processes: a short-time reorientation process which followed a power law relation and a second long-time reorientation

process which followed an exponential relation. Both these processes were strongly affected by the chain stiffness and the chain length. In contrast, it was found that the local structure of the melt was not changed greatly by variation in the parameters of the molecule.

Using the same Brownian dynamics technique, with a harmonic bond potential rather than a FENE and torsional potential, Abrams and Kremer [AK01, AK02] investigated confined and bulk systems of linear molecules where the ratio of bond length to the bead diameter l_0/d_0 was varied. They found that as the bond length increased when compared with the bead diameter, there was an increase in the pressure and surface tension. By examining the local structure of the fluid by calculating radial distribution functions, Abrams and Kremer found that the local ordering in the fluid was enhanced by an increase in the ratio l_0/d_0 . They used this to explain the increase in macroscopic variables. In the subsequent paper [AK02] where the correlation function of the Rouse modes were investigated, they found that when the ratio l_0/d_0 was doubled there was a twenty fold increase in the monomer friction coefficient ζ . This was again attributed to the increase in local ordering in the fluid.

This and the last section have shown that there is considerable interest in the FJC and FENE models for the simulation of polymer melts. Thus a comparison of the molecules is at least worthwhile and has never been attempted to date. The following sections give a brief review of relevant investigations of polymer melts which employed other molecular potentials. We also review several works where the molecular potentials were systematically varied to investigate the effect of this on the properties of the liquid.

4.3 Simulation details

We have compared the results from simulations of 2,4,10 and 50-site monodisperse systems of FENE and FJC molecules under both PCF and PEF. We have also simulated 100-site FENE molecules under both flows. The number of molecules in each system and the range of strain rates simulated are presented in Table 4.1. The simulations were performed using the molecular SLLOD algorithm, the Lees-Edwards pbc's for PCF and the Kraynik-Reinelt pbc's for PEF; these have been described in the previous chapter. The equations of motion were integrated using a fourth order Gear predictor-corrector algorithm [AT87, Gea71] with a time step of $\Delta t = 0.001$ for all systems. To improve the efficiency of the force calculation, a neighbour list algorithm was used as well as a cell method. These algorithms are described for PCF by Allen and Tildesly [AT87] and for PEF by Matin *et al.* [MDT03].

Data presented in this thesis was collected from simulations run at the reduced molecular temperature $T = 1.0$ and bead number density $\rho = 0.84$. Systems were initialised at a low density with beads on an FCC lattice. The systems were allowed to relax away from the lattice at this low density and were then compressed using a bulk compression algorithm [EM90]. For some systems it was necessary to perform further equilibration at an intermediate density before compressing the system to the target density, at which the remainder of the simulations were performed.

We initially performed simulations of the FENE molecules so that we could obtain a comparable bond length for the subsequent simulations of the FJC molecules. The bond length that we chose was $b = 0.97$. Further details of this calculation can be found in the following section (Section 4.4).

For 2,4,10 and 50-site molecules each system was equilibrated at a set strain-rate for between 3.2×10^6 and 6.4×10^6 time-steps to ensure that system had reached a steady state. For 100-site molecules this equilibration was extended to 4×10^7 time-steps. For the data that we present in this

chapter the results were calculated in the following way: every 25 time-steps the instantaneous value of a property was calculated; every 100 time-steps the average of the previous four values was printed to a file; after 4×10^5 time-steps this series was divided into 10 blocks and a block average, a total average and a standard error were calculated. In the case of 2, 4, 10, 20 and 50-site systems, to further improve the statistics, the results of 4 consecutive simulations were averaged and a standard error calculated, this gave the final results which are presented here. For 100-site systems, an average and standard error was calculated from 100 consecutive simulations. The length of the simulations was also governed by requirements of the calculation of diffusion coefficients. Discussion of this is left to the next chapter.

| N_s | N_m | Π_{min} | Π_{max} |
|-------|-------|--------------------|--------------------|
| 2 | 500 | 1×10^{-4} | 5.12 |
| 4 | 500 | 1×10^{-4} | 5.12 |
| 10 | 500 | 1×10^{-5} | 1.0 |
| 20 | 500 | 1×10^{-6} | 5×10^{-1} |
| 50 | 256 | 1×10^{-7} | 5×10^{-2} |
| 100 | 108 | 1×10^{-7} | 1×10^{-3} |

Table 4.1: Some details of systems simulated.

Units

Results are presented in terms of reduced units *i.e.* in terms of the Lennard-Jones coefficients $\epsilon_{LJ}, \sigma_{LJ}$ and the mass of a bead m ; temperature is measured in terms of units k_B/ϵ_{LJ} . The conversion from real units to reduced units gives: the reduced density $\rho^* = \rho/\sigma_{LJ}^3$, the reduced temperature $T^* = k_B T/\epsilon_{LJ}$, reduced time $t^* = (\epsilon_{LJ}/m\sigma_{LJ}^2)^{1/2}t$, reduced pressure $p^* = p\sigma_{LJ}^3/\epsilon_{LJ}$, reduced strain-rate $\dot{\gamma}^* = (m\sigma_{LJ}^2/\epsilon_{LJ})^{1/2}\dot{\gamma}$, reduced viscosity $\eta^* = (\sigma_{LJ}^4/m\epsilon_{LJ})^{1/2}\eta$. For the remainder of the thesis the asterisk is dropped. In the case when simulations are compared with experiments, the Lennard-Jones coefficients can be chosen to fit experimentally observed properties of

the liquid. In our simulations we set $\epsilon_{LJ} = \sigma_{LJ} = m = 1.0$. This choice of units is convenient for simulations because length and time scales are within a numerically manageable range [AT87].

4.4 Bond length calculation

The FENE potential allows the bond length between adjacent sites along the molecule to fluctuate. Thus to perform a comparison between the FENE and FJC molecules we needed to choose a suitable bond length for the FJC molecules.

After simulation of the FENE systems we calculated the mean and variance of bond lengths within the final configurations for each system. The number of bonds in the system ranged from 500 for the 2-site systems to 12544 for the 50-site systems. Data from these calculations are plotted in Fig. 4.1. The error-bars in this figure are the standard deviation of bond lengths. We see that as the strain rate is increased the mean bond length increases only slightly for the shorter molecules. However for the 50-site and 100-site molecules in PEF we see considerable stretching. The variance seen in the FENE bond length is not present in the FJC molecules; this is the main distinction between the two molecules. From these data we obtained a mean bond length over all systems of $\bar{b} = 0.970(8)$. This average value can be compared with the minimum of the bonding potential $b_{min} = 0.9608$, shown in Fig. 3.2. If the approximation is made that the only potential in the system is this bonding potential, then we find numerically that the Boltzmann distribution

$$Prob(b) \propto 4\pi b^2 \exp((U_{WCA}(b) + U_{FENE}(b))/k_B T) \quad (4.1)$$

gives an average bond length of $b_B = 0.9701$ and a standard deviation $\Delta b_B = 0.0334$. This value does not include intramolecular contributions

from non-bonded sites, nor does it include any intermolecular interactions. Note that variance of the bond length is skewed above the mean with little deviation below $b = 0.93$. This is due to the steep repulsive potential during contraction of the bond.

Previous investigations of FJC systems [MDT00, MDT03, DMT03, DMT07] used a value of $b_{FJC} = 1.0$. Looking at Fig. 4.1 this value is approximately one standard deviation greater than the value seen in FENE systems with $\Pi < 10^{-4}$. Though we could have chosen an individual FJC bond length for each strain rate, for convenience we have used just the single value of $b_{FJC} = 0.97$ corresponding to the mean value of the FENE bond length.

4.5 Results

4.5.1 Rheological properties

In this section we compare the rheological properties of the FENE and FJC molecules. These are properties which are directly derived from the stress tensor. We include the shear and extensional viscosities η and $\bar{\eta}$ and the various normal stresses, which have been introduced in Chapter 2 (see Section 2.3). We have also made some comparison with the Curtiss-Bird and Doi-Edwards models.

Extensional and shear viscosity

We have calculated the steady state shear and extensional viscosities for both FENE and FJC molecules. These functions are given in terms of the pressure tensor by

$$\eta = \frac{P_{xy} + P_{yx}}{2\dot{\gamma}} \quad (4.2)$$

and

$$\bar{\eta} = \frac{P_{yy} - P_{xx}}{4\dot{\epsilon}} \quad (4.3)$$

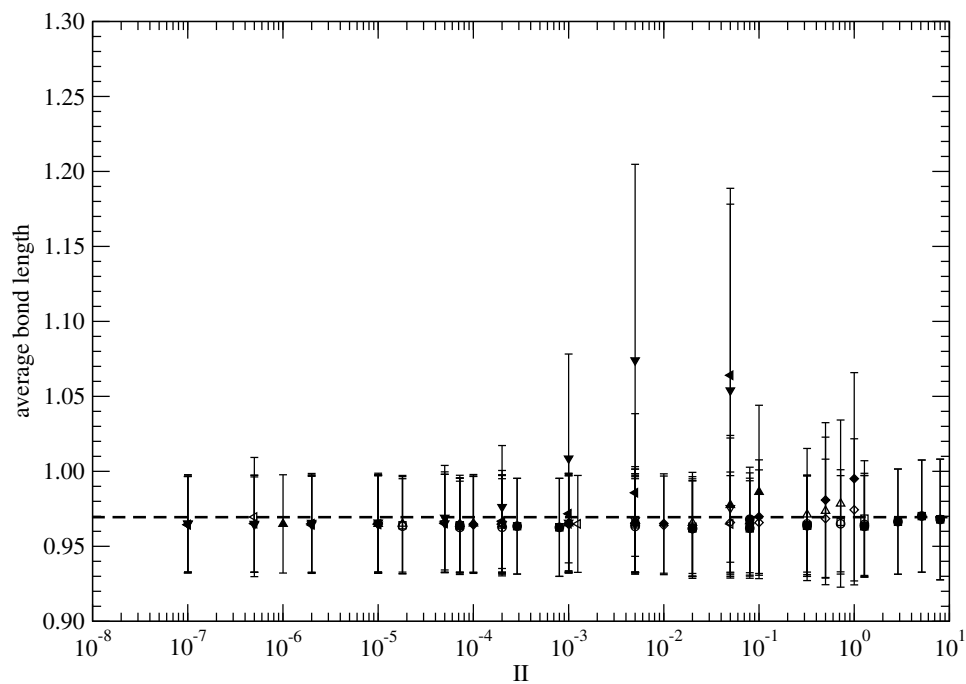


Figure 4.1: Comparison of the average FENE bond lengths in PCF (open symbols) and PEF (closed symbols). The horizontal dashed line corresponds to $\bar{b} = 0.97$. The symbols correspond to 2-site systems (circles), 4-site systems (squares), 10-site systems (diamonds), 20-site systems (triangles-up), 50-site systems (triangles-left), 100-site systems (triangles-down).

respectively. These functions are plotted against the second scalar invariant II in Figs. 4.2 and 4.3 respectively. The second scalar invariant is given for PCF by $II = 2\dot{\gamma}^2$ and for PEF by $II = 8\dot{\epsilon}^2$. This variable is proportional to the rate of viscous heat dissipation in the system at steady state and therefore we are more easily able to compare systems under different flow which are in a similar nonequilibrium state. From the data presented in the two figures we see that the viscosities of the FENE and FJC molecules are very similar. In Fig. 4.3 we see for longer molecules the characteristic increase and plateau in $\bar{\eta}$. For simulations at constant volume the viscosity then begins to increase again. However, Daivis *et al.* [DMT03] have found that if the simulations are performed with constant P_{zz} that the viscosity decreased after the plateau. The shear viscosity for longer molecules (Fig. 4.2) shows that in PCF shear-thinning occurs independent of the molecular weight.

As the strain-rate decreases the systems approach the zero strain-rate viscosity. To estimate the zero strain-rate viscosities for the two molecules we have performed least-squares fits to the viscosity. The functional forms that we used for this were, $y = A + Bx$, $y = A + Bx^2$ and $y = A + Bx^{1/2}$, where the pair (x, y) is $(\dot{\gamma}, \eta)$ and $(\dot{\epsilon}, \bar{\eta})$ for PCF and PEF respectively. The parameter A corresponds to the zero strain-rate viscosity. For each system and functional form we used four to eight data points of lowest strain rate and chose the fit which gave the highest regression coefficient. We then averaged the zero strain-rate viscosity (A) to give the estimates of η_0 and $\bar{\eta}_0$ presented in Table 4.2. We see from these data that for the shorter molecules under PCF the viscosity of the FJC system is larger than the viscosity of the FENE system. Under PEF this trend is reversed with FJC viscosity less than FENE viscosity. Including data for all flows, the difference between the viscosities for FENE and FJC molecules as a percentage of their average value varies between 3% for 2-site molecules under PCF and 22% for 10-

site molecules under PCF; there is no clear trend in the overall variation with molecular weight. For 100-site systems we have estimated $\bar{\eta}_0$ with the extensional viscosity at $\dot{\Gamma} = 1 \times 10^{-7}$. This probably gives an over-estimate of $\bar{\eta}_0$ for 100-site molecules.

In Fig. 4.4 we have plotted the zero strain-rate viscosity against the length of the molecule N_s . In Section 2.5.2 of Chapter 2 we discussed that these data should follow the relationship

$$\eta_0 = \mu N^\nu, \bar{\eta}_0 = \mu N^\nu, \quad (4.4)$$

where $N = N_s - 1$ is the number of bonds in the molecule. The parameters of the least-squares fit to the viscosity data for 10-site to 50-site molecules are given in the second last row of Table 4.2 and the fit to data for 10-site to 100-site molecules is given in the last row of Table 4.2. The average of the exponent over all systems for the range 10-site to 50-site is $\nu = 0.93(9)$. The best fit for PCF data with systems in the range 10-site to 100-site gives the exponent $\nu = 1.08(3)$. This is very close to the expected value $\nu = 1.0$ as predicted by the Rouse model and found by Kröger and Hess [KH00] in their simulations of FENE molecules. The greatest difference between FENE and FJC is seen in the exponent ν calculated for the range 10-site to 50-site; the FJC systems having a smaller exponent ($\nu = 0.84(3)$) than the FENE molecules ($\nu = 1.09(3)$). It should be noted that a fit to systems in the range 2-site to 50-site gives a much smaller exponent, $\nu \approx 0.77$. 2-site molecules do not exhibit Rouse behaviour, and thus the inclusion of these molecules in the calculation of ν leads to its decreased value.

Normal stress differences

Data for the steady state first (Ψ_1) and second (Ψ_2) normal stress coefficients under PCF are presented in Figs. 4.5 and 4.6 respectively. We have intro-

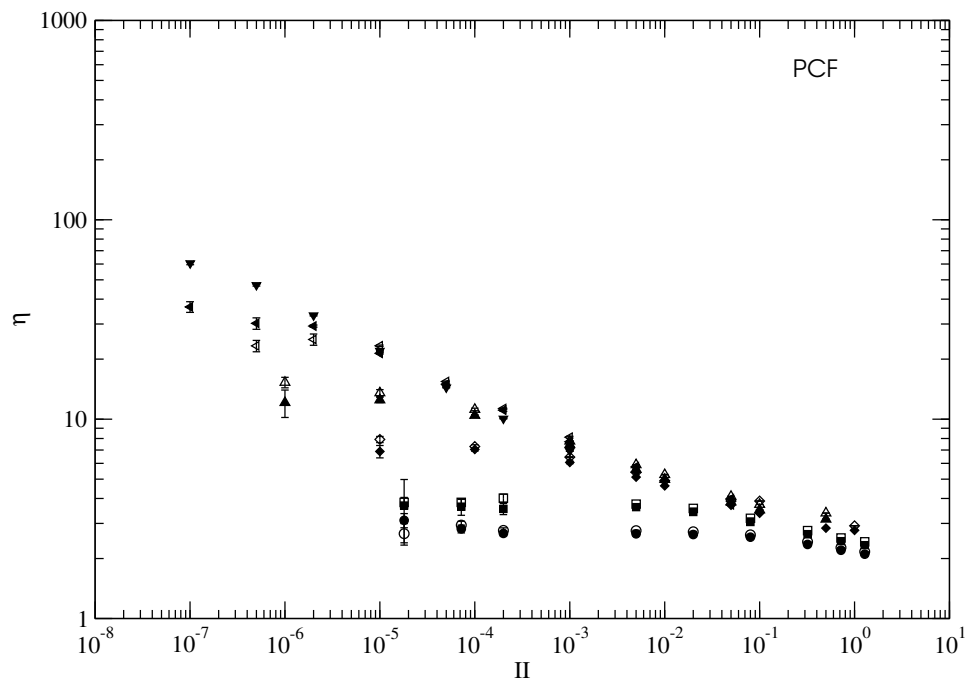


Figure 4.2: Comparison of the shear viscosity η for FJC molecules (open symbols) and FENE molecules (closed symbols). The symbols correspond to 2-site systems (circles), 4-site systems (squares), 10-site systems (diamonds), 20-site systems (triangles-up), 50-site systems (triangles-left), 100-site systems (triangles-down).

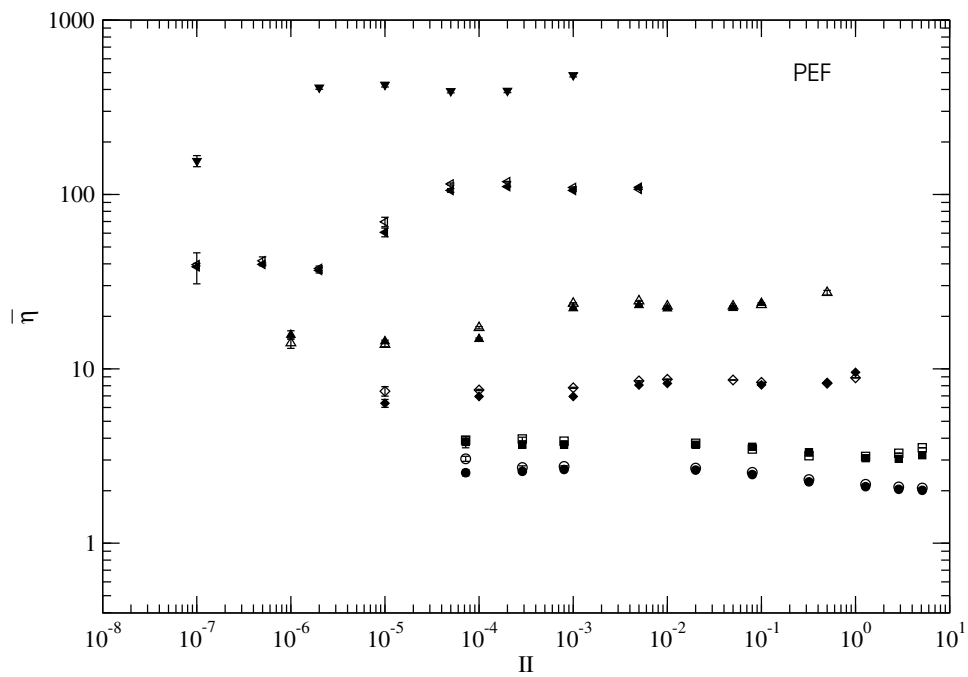


Figure 4.3: Comparison of the extensional viscosity $\bar{\eta}$ for FJC and FENE molecules of length 2,4,10,20 and 50 monomers. We have included just FENE molecules for the 100-site systems. The symbols are the same as in Fig. 4.2.

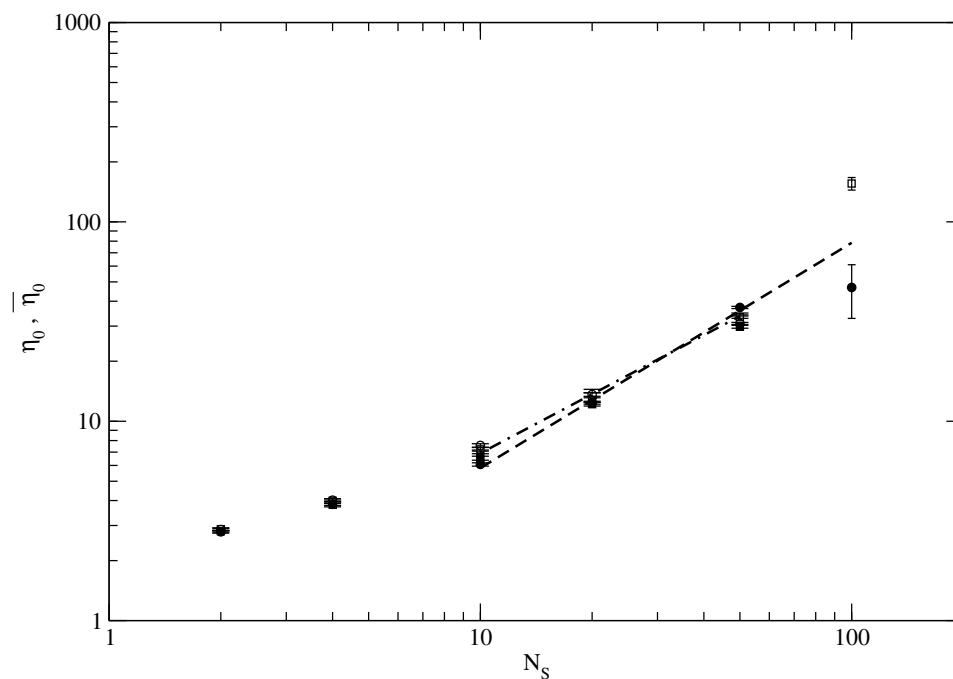


Figure 4.4: Comparison of the zero strain-rate viscosity for PCF (circles) and PEF (squares). Open symbols correspond to FJC molecules, closed symbols correspond to FENE molecules. The dashed line (---) is the best fit to the 10-site to 100-site PCF data ($\eta_0 = 0.87(N_s - 1)^{0.93}$). The dot-dashed line (- · - ·) is the best fit to the 10-site to 50-site data averaged over all systems ($\eta_0 = 0.54(N_s - 1)^{1.08}$).

| Flow Molecule | PCF | | PEF | |
|-----------------|----------------------|---------------------|----------------------|----------------------|
| | FENE η_0 | FJC η_0 | FENE $\bar{\eta}_0$ | FJC $\bar{\eta}_0$ |
| 2-site | 2.79(4) | 2.86(4) | 2.81(3) | 2.87(5) |
| 4-site | 3.83(1) | 4.02(7) | 3.82(4) | 3.99(4) |
| 10-site | 6.1(1) | 7.6(2) | 6.5(2) | 7.2(2) |
| 20-site | 12.4(2) | 13.6(3) | 12.2(3) | 12.8(3) |
| 50-site | 37.2(5) | 30.9(4) | 29.8(5) | 33.3(4) |
| 100-site | 50(10) | - | 160(10) | - |
| 10 to 50-sites | $0.54(5)N^{1.09(3)}$ | $1.2(1)N^{0.84(3)}$ | $0.88(8)N^{0.90(5)}$ | $0.94(7)N^{0.91(5)}$ |
| 10 to 100-sites | $0.54(5)N^{1.09(3)}$ | - | $0.73(6)N^{0.97(5)}$ | - |

Table 4.2: Comparison of the zero strain-rate viscosities η_0 and $\bar{\eta}_0$ for FENE and FJC molecules extrapolated from the finite strain-rate viscosities. The last two rows give the least-squares fit parameters for η_0 , $(\bar{\eta}_0) = \mu N^\nu$ using the 10-site to 50-site data and 10-site to 100-site data ($N = N_s - 1$).

duced these functions in Chapter 2, however, for convenience we reintroduce them here,

$$\Psi_1 = \frac{P_{yy} - P_{xx}}{\dot{\gamma}^2}$$

$$\Psi_2 = \frac{P_{zz} - P_{yy}}{\dot{\gamma}^2}.$$

These functions measure the difference between stresses normal to the faces of a cubic volume of fluid. It had been suggested (the Weissenberg Hypothesis [Wei47, BAH87]) that the second normal stress in fluids is zero, however it is now known that the Ψ_2 is about 10% of the value of Ψ_1 . From the simulation data it is seen that both functions decrease in value as the strain rate is increased. In general these functions show an increase with molecular length, which is comparable with viscosity. However in comparison with the shear viscosity, the range of Ψ_1 is about an order of magnitude greater, particularly for longer molecules. The statistical variance in these data is considerable, especially for Ψ_2 . The ratio $-\Psi_1/\Psi_2$ (Fig. 4.7) has a large

variance as a consequence of the variance in both terms. From these data we can only estimate the ratio at being between 0.1 and 1.0 for most systems. The difference between the data for FENE and FJC is also greatest for these quantities. However, without better statistics we are unable to make any stronger conclusions about this difference.

Under extensional flows, the first and second extensional viscosities are

$$\eta_1 = \frac{P_{yy} - P_{xx}}{\dot{\epsilon}} \quad (4.5)$$

and

$$\eta_2 = \frac{P_{yy} - P_{zz}}{\dot{\epsilon}} \quad (4.6)$$

respectively. Again these have already been introduced in Chapter 2, and the first extensional viscosity η_1 is proportional to the extensional viscosity ($4\bar{\eta} = \eta_1$) and therefore we do not discuss it further here. Data for the second extensional viscosity η_2 are presented in Fig. 4.8. Daivis *et al.* [DMT03] note that this function has been measured only rarely and cite just Wagner *et al.* [WBH⁺00] who measure the transient value of this function. Comparing with other viscometric functions for PEF and PCF we note that there is less variation with molecular weight for this function. η_2 decreases and then has a small region of increase at large strain rates. As for the viscosity, this increase did not occur when simulations were performed with constant P_{zz} by Daivis *et al.* [DMT03]. The ratio η_2/η_1 is presented in Fig. 4.9. These functions have better statistics than the normal stress coefficients for PCF. We see that the ratio approaches the value 1/2 for low strain rates and has a larger value for short molecules. Matin [Mat01] explains this property by noting that in the Newtonian regime, P_{zz} does not change, and the positive change in P_{yy} is equal in magnitude to the negative change in P_{xx} . It is seen from this ratio that for larger molecules η_1 dominates η_2 and there is a region over which the ratio is approximately constant. In each of the

functions described here there is little variation between the values for FENE and FJC molecules.

Comparison with the Curtiss Bird model

There have been several publications where comparison has been made between molecular dynamics simulations, the Rouse model and the model of Doi and Edwards. Some of these have aimed to observe reptative diffusion, some have calculated the correlation functions for the Rouse modes while others have simply looked for the onset of the reptative regime in both rheological properties and the self-diffusion of molecules in the melt.

In this work we have only been able to perform some simple comparisons of the predictions of the model with the rheological predictions of NEMD simulation. In the next chapter some comparison is made with the diffusion data.

Comparison of the extensional viscosity data (Fig. 4.3) with the CB-model (Fig. 2.9) would suggest that the steady state prediction of the CB-model might be fitted to the viscosity data from NEMD simulation. Note that some care should be taken in comparing these figures since in Fig. 2.9 the ratio has been plotted on a linear scale. For the longer molecules the steady state viscosity which has been calculated from simulation starts at the zero strain rate viscosity increasing through an inflection point and reaching a plateau value $\bar{\eta}_\infty$ at high strain rates. This plateau viscosity has been calculated above in Section 4.5.1. By comparison, for values of the link tension coefficient ϵ greater than approximately 0.5 the CB-model has very similar behaviour and provides a plateau viscosity which might be fitted to the simulation data.

The family of functions presented in Fig. 2.9 have two parameters: the time scale λ and the link tension coefficient ϵ . We have not performed a full least-squares fit of the CB-model. Rather, with the value of the plateau

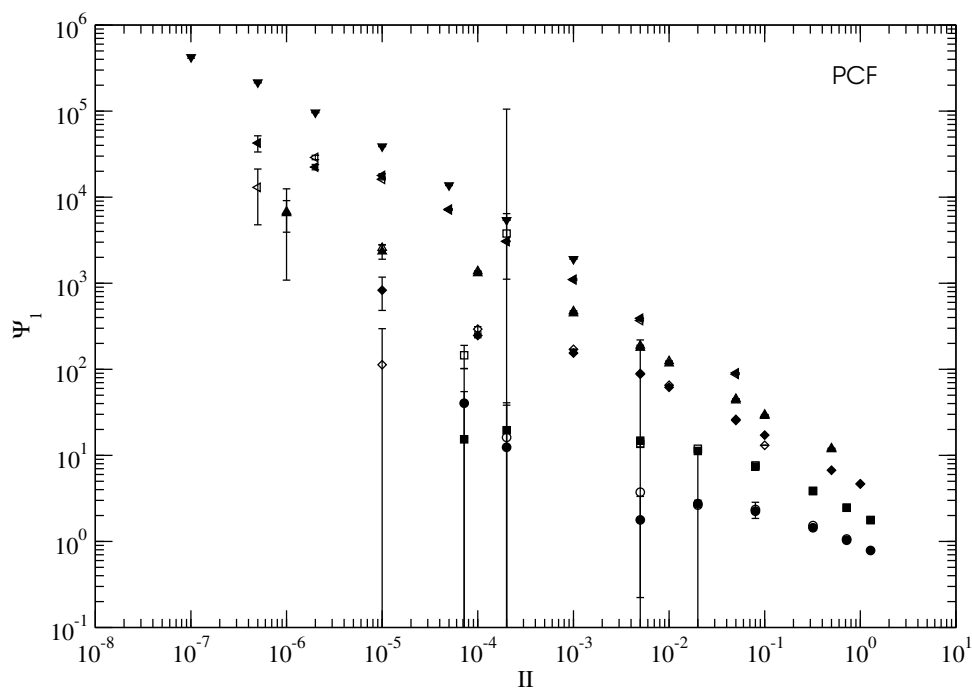


Figure 4.5: First normal stress Ψ_1 for FJC and FENE molecules of length 2,4,10,20 and 50 monomers. We include data for 100-site FENE molecules. The system is under shear flow (PCF). The symbols are the same as in Fig. 4.2.

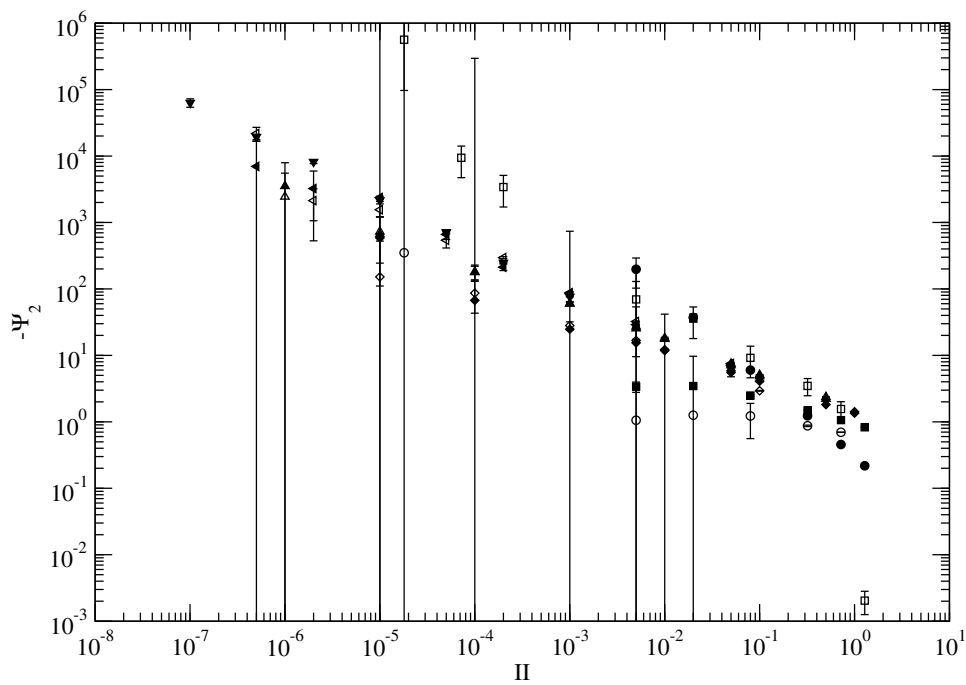


Figure 4.6: Second normal stress $-\Psi_2$ for FJC and FENE molecules of length 2,4,10,20 and 50 monomers. We include data for 100-site FENE molecules. The system is under shear flow (PCF). The symbols are the same as in Fig. 4.2.

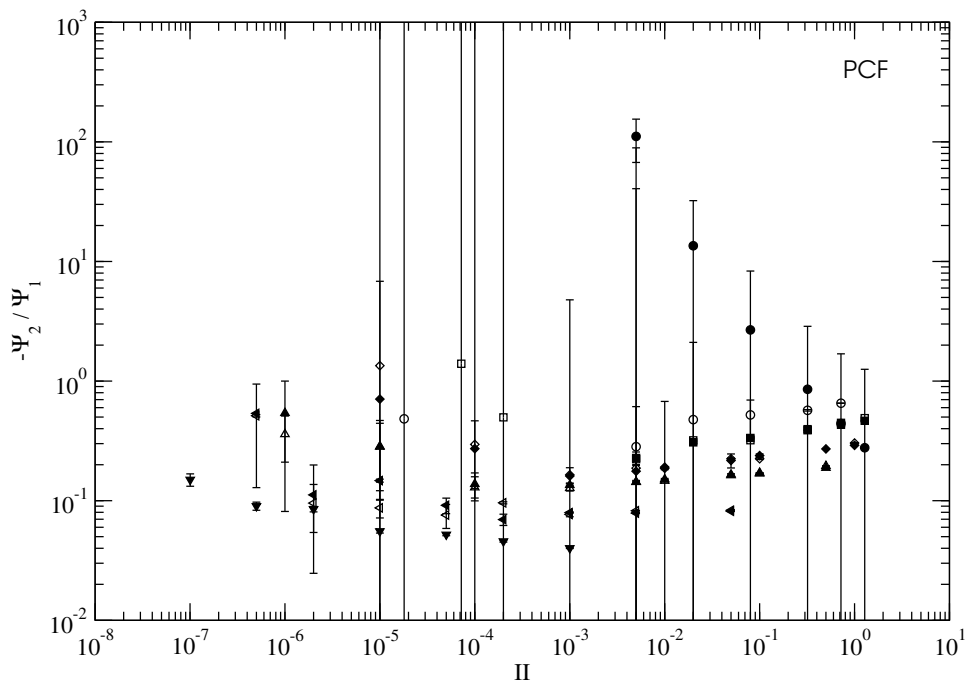


Figure 4.7: The ratio of the normal stresses $-\Psi_2/\Psi_1$ for FJC and FENE molecules of length 2,4,10,20 and 50 monomers. We include data for 100-site FENE molecules. The system is under shear flow (PCF). The symbols are the same as in Fig. 4.2.

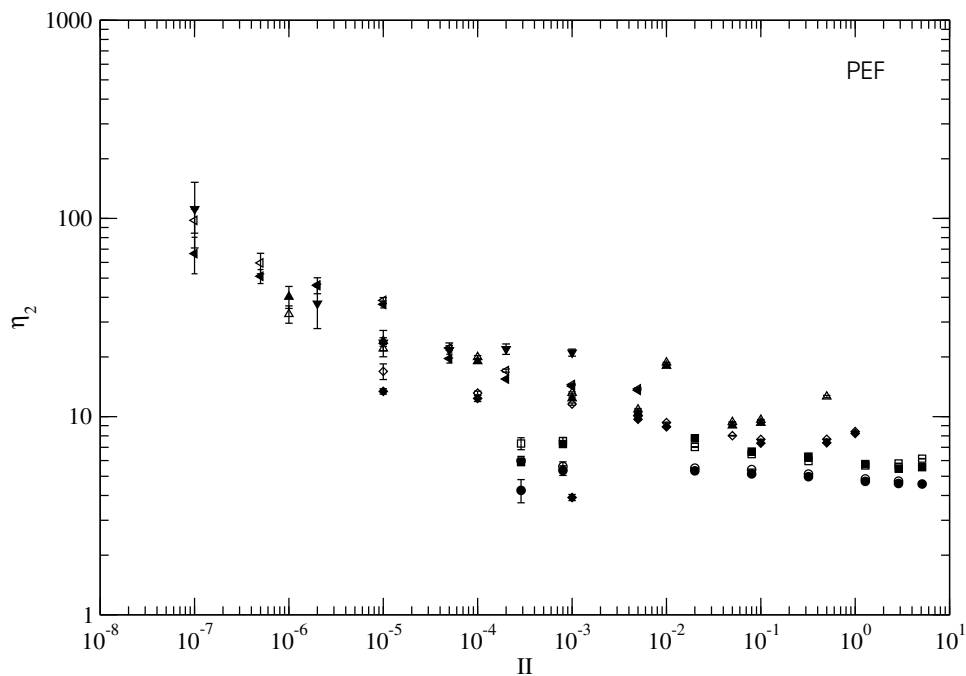


Figure 4.8: Second normal stress η_2 for FJC and FENE molecules of length 2,4,10,20 and 50 monomers. We include data for 100-site FENE molecules. The system is under extensional flow (PEF). The symbols are the same as in Fig. 4.2.

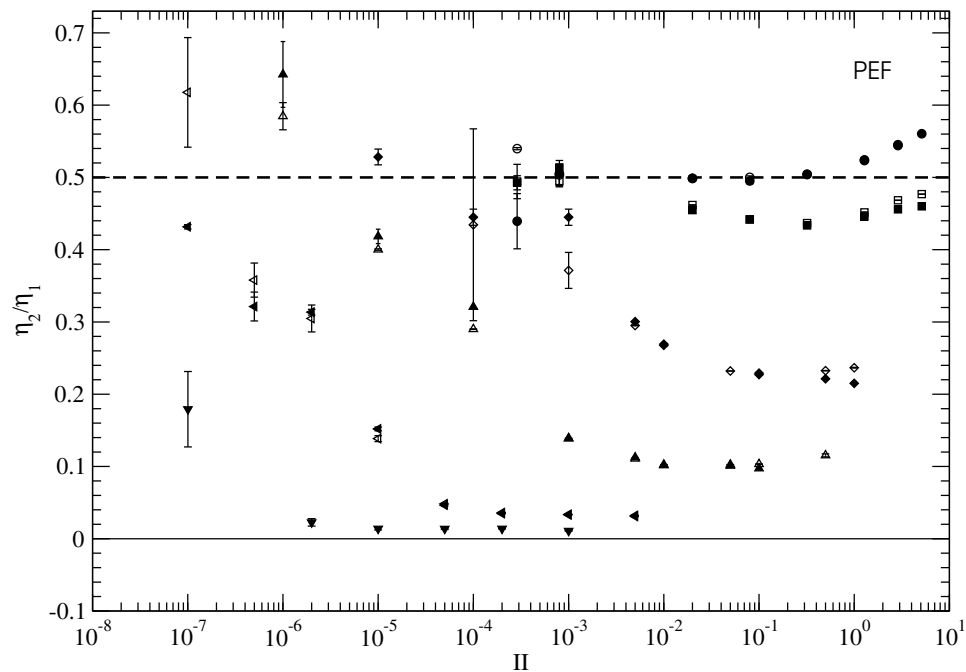


Figure 4.9: The ratio of the normal stresses η_2/η_1 for FJC and FENE molecules of length 2,4,10,20 and 50 monomers. We include data for 100-site FENE molecules. The system is under elongational flow (PEF). The symbols are the same as in Fig. 4.2.

viscosity calculated above, we have used (2.82), which does not require λ , to obtain an expression for the link tension coefficient,

$$\epsilon = \frac{6(\bar{\eta}_\infty/\bar{\eta}_0)}{15 - 4(\bar{\eta}_\infty/\bar{\eta}_0)}. \quad (4.7)$$

Values for the ratio $\bar{\eta}_\infty/\bar{\eta}_0$ together with the calculated value of ϵ are presented in Table 4.3 for systems of 20-site and 50-site molecules. For the 100-site data we have used $\bar{\eta}_0$ calculated from the PCF data, all others have been calculated using PEF data. Comparing the model and simulation data

| Molecule | | $\bar{\eta}_\infty/\bar{\eta}_0$ | ϵ |
|----------|------|----------------------------------|------------|
| 20-site | FENE | 1.87(7) | 1.5(1) |
| 20-site | FJC | 1.83(6) | 1.4(1) |
| 50-site | FENE | 3.6(1) | 40(40) |
| 50-site | FJC | 3.4(1) | 14(6) |
| 100-site | FENE | 9(3) | -2.7(6) |

Table 4.3: Calculation of the link tension coefficient ϵ of the Curtiss-Bird model in the pure reptation approximation, using equation 4.7 and NEMD data presented in Fig. 4.3.

gives an estimate for the link tension coefficient which is found to be outside the range $0 \leq \epsilon \leq 1$, allowed by the model (see Assumption 2 on page 42). In particular for the 100-site system ϵ is negative because $\bar{\eta}_\infty/\bar{\eta}_0 > 15/4 = 3.75$. Error bars in the 50-site data are large because the ratio of viscosities is close to 3.75.

From these data it must be concluded that the model, as we have presented it, is not valid for the situation we consider here. However, calculations made in Chapter 2 were only possible because we made the assumption that the system was in the pure reptation limit, with the reptation coefficient $\epsilon' = 0$. This assumption is probably the main source of error in the comparison that we make here. This is the case because Kröger and Hess [KH00] have found that reptation only becomes dominant in systems with

N_s greater than one hundred. It should however be noted that even for 100-site systems it is found that $\bar{\eta}_\infty/\bar{\eta}_0 > 1.5$. Further investigation of this inconsistency would require simulation of larger molecules or the calculation of the CB-model away from the pure reptation regime. Another observation also needs to be considered; in the simulation prediction it is found that for simulations at constant volume, beyond the plateau region a sharp increase in the viscosity is observed. Simulation with constant P_{zz} leads to an observed decrease in the viscosity after the plateau region [DMT03]. This last observation is consistent with results from experiment, however, the CB-model would only account for this if the plateau region was ignored. The Doi-Edwards prediction, which corresponds to the lowest curve in Fig. 2.9 ($\epsilon = 0$), clearly shows that this model can not be used to predict the results for the longer molecules. Again in this case it may be, that for constant pressure systems of longer molecules, the plateau ratio is much smaller and therefore the Doi-Edwards prediction could be fitted to the decreasing viscosity which is seen in these systems.

Further investigation may also consider the asymptotic form of the steady state viscosity under PCF. The prediction of the CB-model in this limit is [KLH93],

$$\lim_{\dot{\gamma} \rightarrow +\infty} \eta(\dot{\gamma}) \sim \epsilon(\lambda\dot{\gamma})^{-1} \quad (4.8)$$

The variation of the coefficient ϵ leads to the family of curves that were presented in Fig. 2.7. The coefficient λ is given in the pure reptation regime by $\lambda = L^2/D$ where L is the molecular length and D is the centre of mass diffusion coefficient. It is assumed that the diffusion coefficient is calculated at equilibrium. By calculating D it would be possible to then calculate ϵ from the the high strain rate behaviour of the viscosity using (4.8).

4.5.2 Microscopic properties

An important feature of molecular simulations is the accessibility of the molecular details of a system, which allows the direct calculation of microscopic properties which in experiment would require sophisticated optical or scattering techniques. In this section we investigate the alignment and extension of molecules in flow, as well as their rotation. Similar calculations of the FJC molecule with $b = 1.0$ under PEF and PCF have been performed by Matin *et al.* [Mat01] for molecules up to 50 sites in length. Calculations for dendrimer and linear FENE molecules under PCF at $T = 1.25$ have also been presented by Boško *et al.* [BTS04a, Boš05]. The data presented here will be used in the next chapter to help explain the behaviour of diffusion in these systems.

Extension of molecules

At equilibrium it is known that the orientation of molecules in a melt is isotropic. However, away from equilibrium, under flow, it is well known that molecules align; this is called Maxwell's effect or flow birefringence. In this section and the next we introduce several measures which give a quantitative indication of the change in conformation of molecules in the system.

For an individual molecule composed of identical particles the tensor of gyration is given by,

$$R_g^2 \equiv \frac{1}{N_s^2} \sum_{\alpha=1}^{N_s} \sum_{\beta=1}^{N_s} (\mathbf{r}_\alpha - \mathbf{r}_\beta)(\mathbf{r}_\alpha - \mathbf{r}_\beta) \quad (4.9)$$

where \mathbf{r}_α and \mathbf{r}_β are the positions of beads α and β respectively. The radius of gyration is defined as $R_g^2 = \text{trace}(R_g^2)$ and as we noted in Chapter 2 it is proportional to the scalar moment of inertia $I_m = MR_g^2$, where M is the total mass of the molecule. In the case here where each of the beads has the same mass, the moment of inertia *tensor* is -1 times the traceless part of

R_g^2 . The gyration tensor was averaged over all molecules in the system and the average radius of gyration squared ($\langle R_g^2 \rangle$) calculated. Results of $\langle R_g^2 \rangle$ are presented in Fig. 4.10 for PCF and in Fig. 4.11 for PEF.

A further indication of the structure within the liquid is provided by calculation of the average mean-squared end-to-end distance $\langle \mathbf{R}_{ee}^2 \rangle$ of molecules. This has again been calculated as an average over the molecules in the system and then as a time average. Results for PCF and PEF are presented in Figs. 4.12 and 4.13 respectively. For large chains, random walk theory predicts $\langle \mathbf{R}_{ee}^2 \rangle = 6\langle \mathbf{R}_g^2 \rangle$ which we can compare with the results here. A brief analysis of the data shows that this relationship holds for systems close to equilibrium. However, it is found that as the molecules stretch at high strain rates that the ratio becomes greater than six.

For the smallest molecules, 2-site and 4-site, there is little variation in $\langle R_g^2 \rangle$ and $\langle R_{ee}^2 \rangle$ for all systems. For the 2-site FJC molecules it is clear that these quantities are necessarily fixed. For the longer molecules (10 to 100-sites) it is seen that both $\langle R_{ee}^2 \rangle$ and $\langle R_g^2 \rangle$ increase with the strain rate except at the highest strain rate for PEF where there is seen to be a slight decrease in these functions. This is attributed to the use of the constant volume algorithm rather than constant pressure algorithm. The plateau value of $\langle R_{ee}^2 \rangle$, at high strain rates, indicates that under PEF molecules become fully extended. For example in the case of 50-site molecules, the full extension of a molecule would correspond to $R_{ee}^2 = (49 \times 0.97)^2 = 2259$ which is close to the observed plateau value. As for the rheological properties, there is almost no variation between FENE and FJC molecules. The observed variation in the FENE bond length, presented above, has little effect since, instantaneously, some bonds will be longer and others shorter.

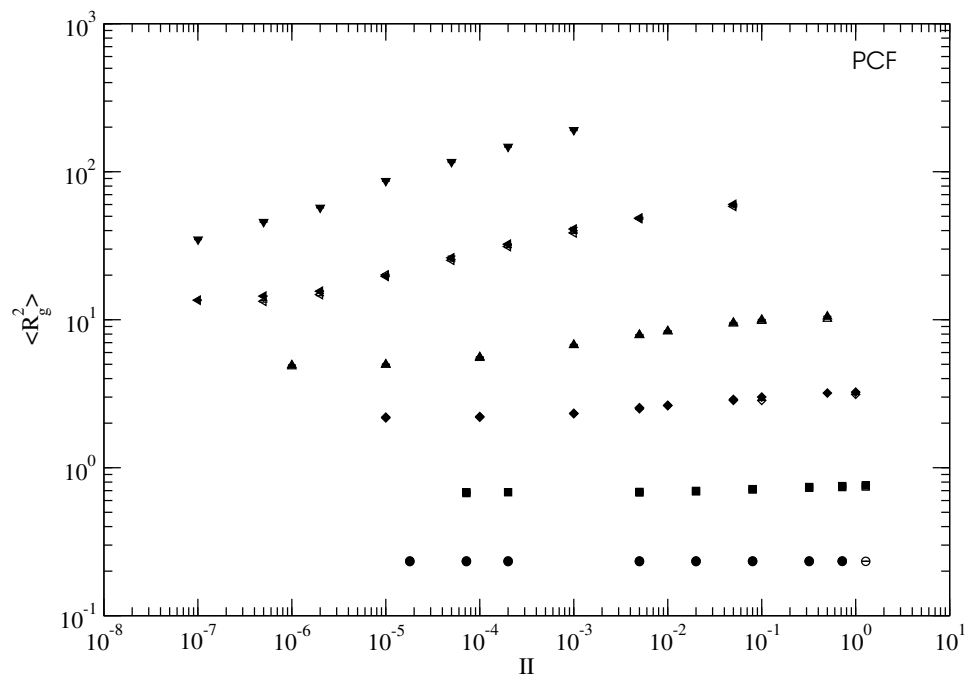


Figure 4.10: Comparison of the mean-squared radius of gyration \mathbf{R}_g^2 for FJC and FENE molecules of length 2,4,10,20 and 50 monomers. We include data for 100-site FENE molecules. The system is under shear flow (PCF). The symbols are the same as in Fig. 4.2.

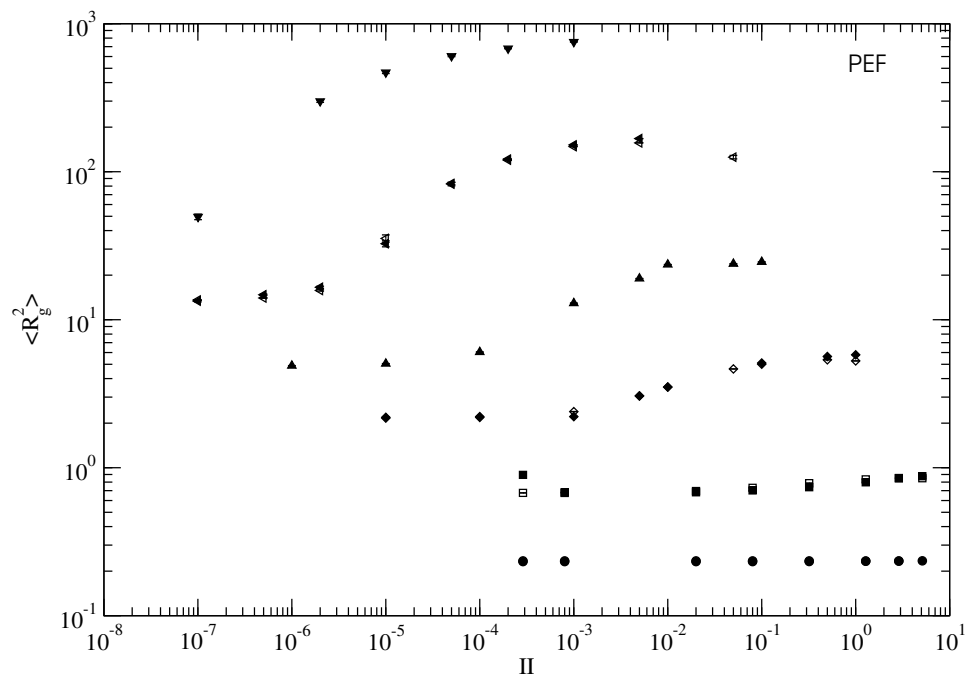


Figure 4.11: Comparison of the mean-squared radius of gyration \mathbf{R}_g^2 for FJC and FENE molecules of length 2,4,10,20 and 50 monomers. We include data for 100-site FENE molecules. The system is under extensional flow (PEF). The symbols are the same as in Fig. 4.2.

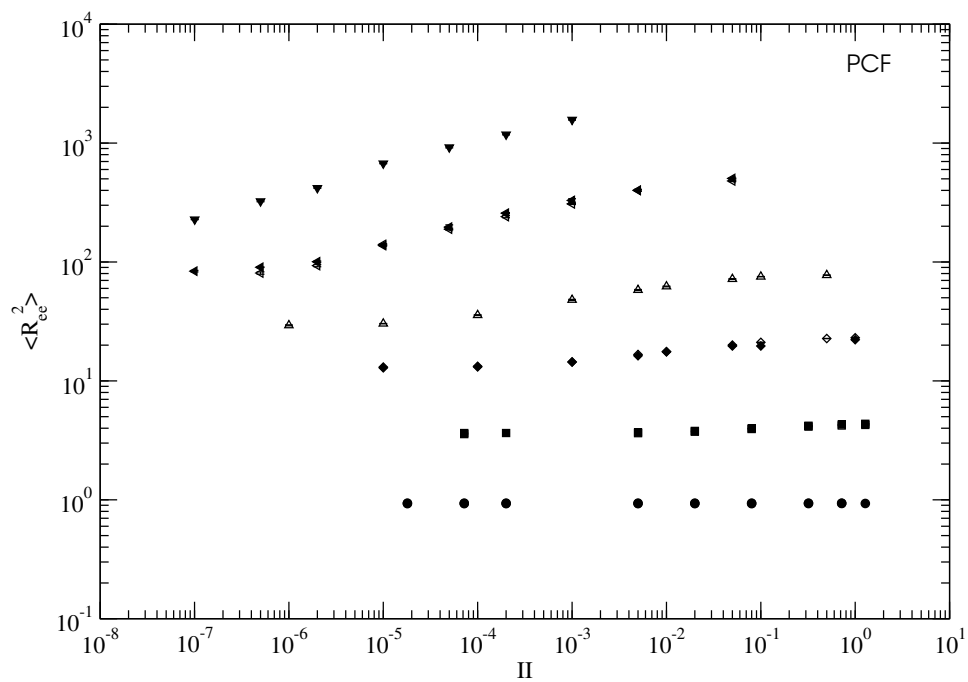


Figure 4.12: Comparison of the mean-squared end-to-end distance \mathbf{R}_{ee}^2 for FJC and FENE molecules of length 2,4,10,20 and 50 monomers. We include data for 100-site FENE molecules. The system is under shear flow (PCF). The symbols are the same as in Fig. 4.2.

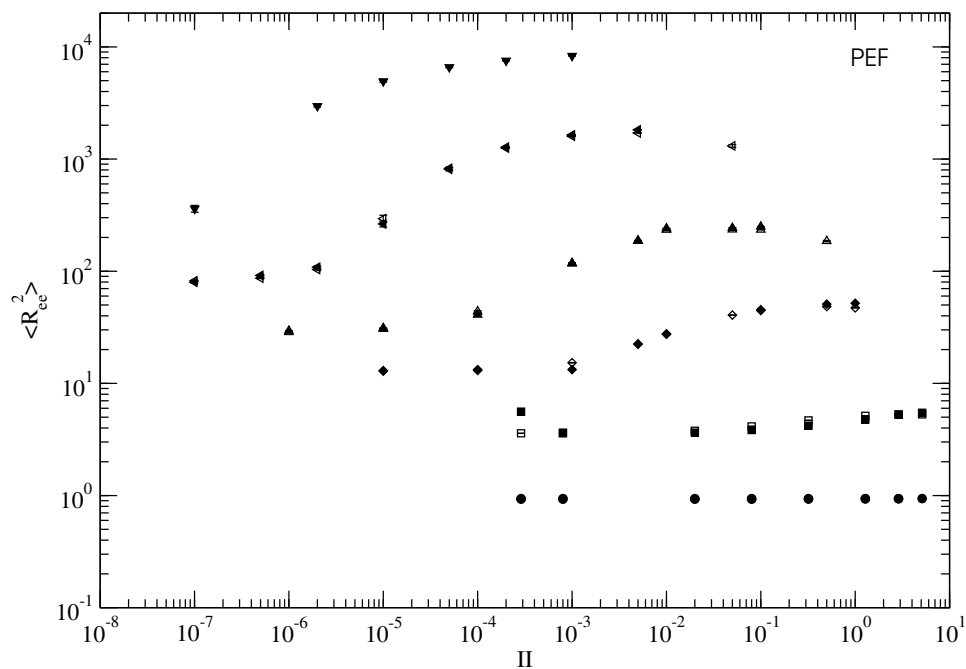


Figure 4.13: Comparison of the mean-squared end-to-end distance \mathbf{R}_{ee}^2 for FJC and FENE molecules of length 2,4,10,20 and 50 monomers. We include data for 100-site FENE molecules. The system is under extensional flow (PEF). The symbols are the same as in Fig. 4.2.

The order tensor

From the gyration tensor we are able to obtain more detail about the alignment in the systems. We have calculated the order tensor \mathbf{S} , which is a symmetric traceless tensor calculated instantaneously during a simulation using the relation,

$$\mathbf{S} = \frac{1}{N_m} \sum_{i=1}^{N_m} (\hat{\mathbf{u}}_i \hat{\mathbf{u}}_i - \frac{1}{3} \mathbf{I}) \quad (4.10)$$

where $\hat{\mathbf{u}}_i$ is the unit vector corresponding to the largest eigenvalue of the gyration tensor for molecule i . This tensor represents a collection of correlation coefficients; each element $S_{\alpha\beta}$ is the correlation between the component $u_{i\alpha}$ and $u_{i\beta}$ of the unit vector for an individual chain. Further discussion of correlation is given in the next chapter (see Section 5.4). The order tensor for tangent vectors along a chain has already been used in the derivation of the stress tensor for the Doi-Edwards model (see (2.55)). In that model it was assumed that the stress tensor was proportional to the order tensor. This relation is known as the stress-optic rule.

From the order tensor one can obtain the order parameter S , which is a single numerical indicator of the alignment in a system. The order parameter is $3/2$ of the largest eigenvalue of the tensor \mathbf{S} , and the corresponding eigenvector is the direction of alignment in the system. The value of S has the range $0 \leq S \leq 1$. When $S = 0$ the molecules are isotropic while when $S = 1$ the molecules are perfectly aligned.

The order parameter for systems under PCF and PEF is presented in Figs. 4.14 and 4.15 respectively. It is seen from both figures that, in general, S increases with the increase of the strain rate. However, there is a distinction between the alignment for PCF and PEF: While for PEF, the order parameter reaches a plateau value and remains at this value over a wide range of strain rates, for PCF a plateau is only reached at very high strain rates and only for longer molecules. It is also seen that for larger molecules

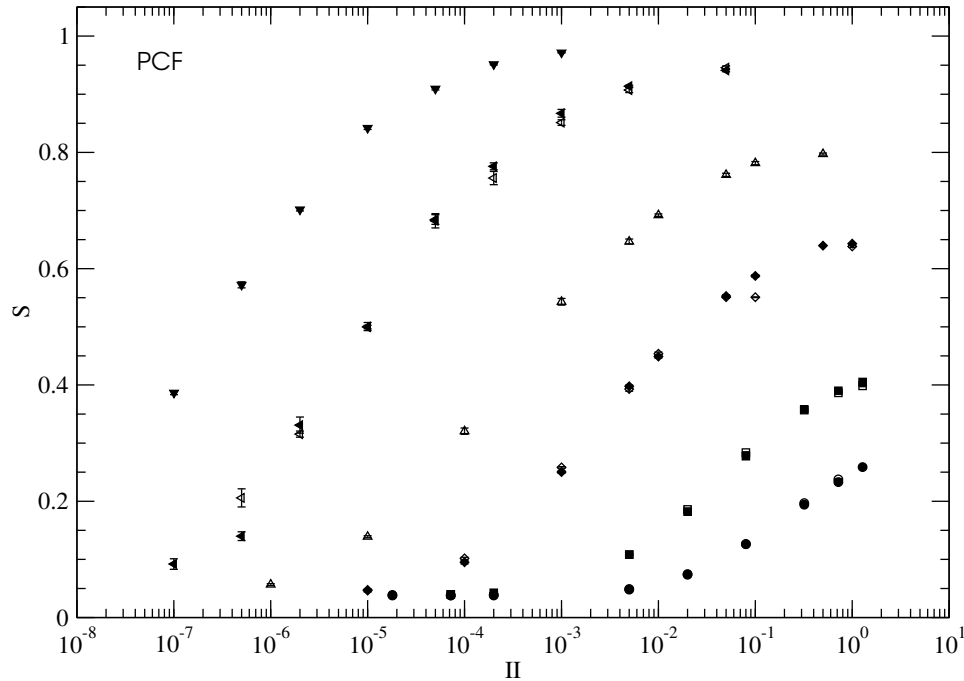


Figure 4.14: Comparison of the order parameter S for FJC and FENE molecules of length 2,4,10,20 and 50 monomers. We include data for 100-site FENE molecules. The system is under shear flow (PCF). The symbols are the same as in Fig. 4.2.

the increase in alignment begins at a lower strain rate and occurs more rapidly. Qualitatively this is similar to the earlier onset of non-Newtonian behaviour for longer molecules. The alignment shows little difference between FENE and FJC systems, however, under PEF in the range where S increases there is greatest variation between the two models. The sensitivity on strain rate in this region would suggest that the uncertainty in these values is greater. For PEF there is also a slight decrease in S at the highest strain rates, which again corresponds to rates where the difference between the constant volume and constant pressure algorithms has been observed by Daivis *et al.* [DMT03].

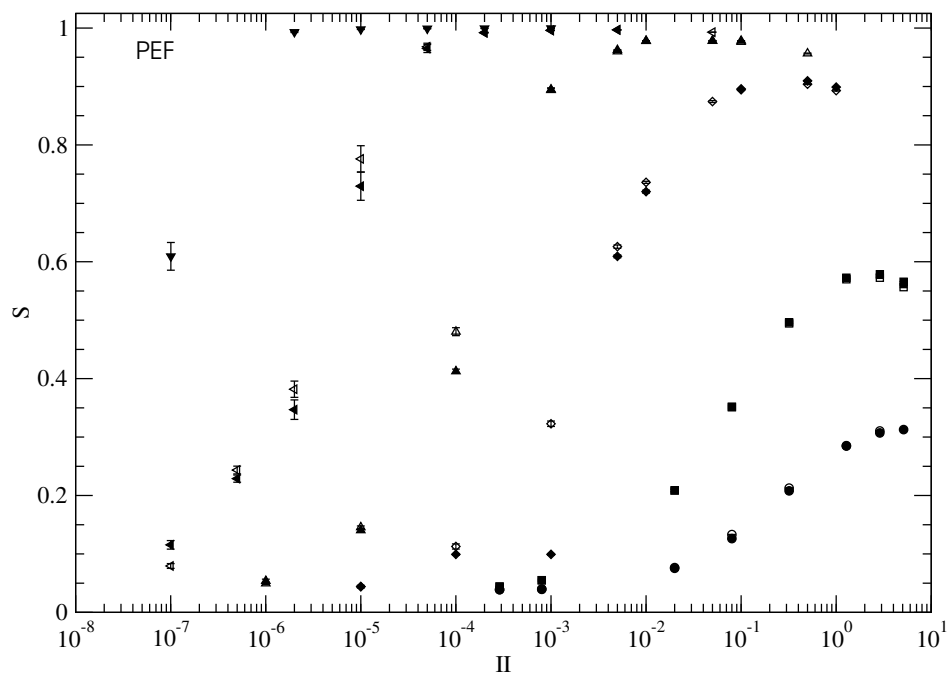


Figure 4.15: Comparison of the order parameter S for FJC and FENE molecules of length 2,4,10,20 and 50 monomers. We include data for 100-site FENE molecules. The system is under extensional flow (PEF). The symbols are the same as in Fig. 4.2.

Alignment angle

From the order tensor one can also calculate the alignment angle (also known as the birefringence extinction angle). This is the angle χ that a molecule makes on average with the x -axis in the xy -plane. If the largest eigenvector of the gyration tensor of a molecule is $\hat{\mathbf{e}} = (e_x, e_y, e_z)$ then in planar flows the z component vanishes ($e_z = 0$) because there is on average no component of alignment in the $\hat{\mathbf{n}}_z$ direction. For this situation we have,

$$\chi = \arctan\left(\frac{e_y}{e_x}\right). \quad (4.11)$$

While for PEF it is known [Mat01] that the alignment is parallel with the x -axis, for PCF in the Newtonian regime molecules align on average with $\chi = 45^\circ$. Results for χ under PCF are presented in Fig. 4.16, and it is seen that in the non-Newtonian regime the alignment angle decreases with the strain rate. At a single strain rate, χ decreases with the molecular length, which is due to the earlier onset of the non-Newtonian regime for longer molecules. It is not explicitly clear from these data that molecules approach the 45° alignment in the Newtonian regime. 100-site molecules only reach $\chi = 20^\circ$ at the lowest strain rate we have considered, 50-site molecules do approach $\chi = 40^\circ$, however, the FENE result for the lowest strain rate has an alignment of approximately $\chi = 55^\circ$. For shorter molecules – 2, 4 and 10-sites – there is a strain rate below which χ diverges significantly from the trend towards alignment at $\chi = 45^\circ$. Comparing with the order parameter in Fig. 4.14 it is clear that at these low strain rates there is less ordering in the fluid, and so a longer simulation is required to obtain a better estimate for the average alignment angle. It is seen once more that there is little difference between FENE and FJC molecules.

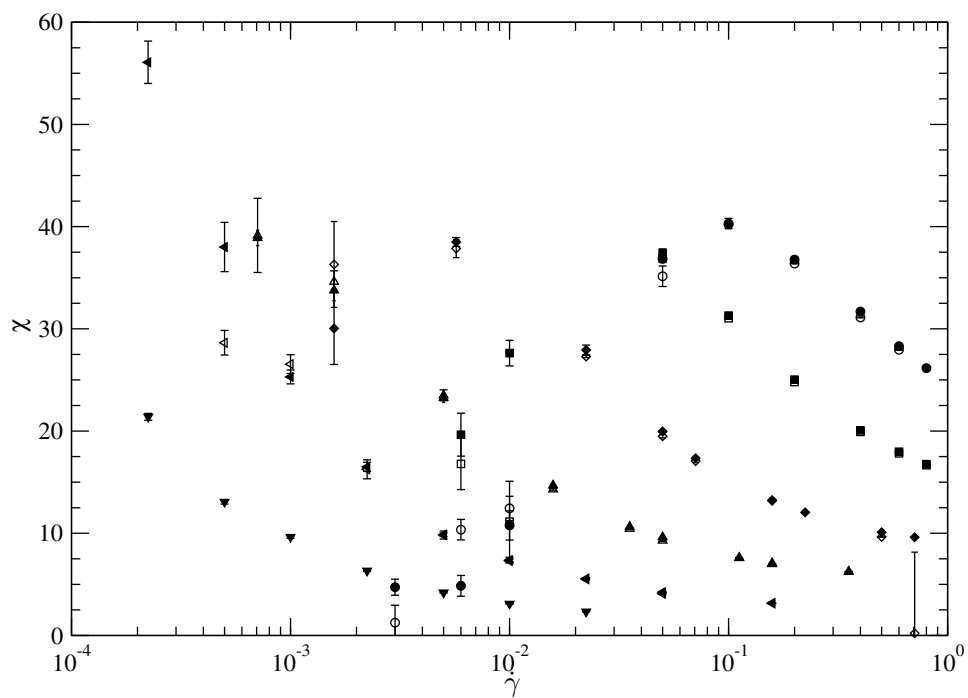


Figure 4.16: The alignment angle χ under PCF. Symbols are the same as in Fig. 4.2.

Spin angular velocity

Despite the alignment of molecules which has been described and calculated in the preceding sections, molecules also undergo rotation in PCF; under PEF it has been found that the average angular momentum for molecules is zero [Mat01]. For PCF it is found that in the Newtonian regime the spin angular velocity of molecules should be $\dot{\gamma}/2$ in the clockwise sense about the $\hat{\mathbf{n}}_z$ direction [EEM87]. The instantaneous angular velocity of molecules is calculated by inverting the relation,

$$\mathbf{L} = \mathbf{I}_m \cdot \boldsymbol{\omega} \quad (4.12)$$

where \mathbf{L} is the angular momentum of the molecule with respect to its centre of mass, \mathbf{I}_m is the moment of inertia tensor and $\boldsymbol{\omega}$ is the angular velocity vector. Once calculated, the components of the instantaneous angular velocity are averaged over the course of a simulation, in a similar way to the preceding properties.

We have confirmed that for PEF all components of the angular velocity are on average zero. Under PCF just the component ω_z is nonzero and values for this component are shown in Fig. 4.17. The line $-\dot{\gamma}/2$ is also plotted in this figure. It is seen that for 4-site to 50-site molecules the angular velocity approaches $-\dot{\gamma}/2$ at low strain rates. This is a relationship which is predicted by irreversible thermodynamics [EEM87] in the steady-state and the limit as $\dot{\gamma} \rightarrow 0$. We have not simulated the 100-site system at small enough strain rates to confirm this behaviour for this system, and the uncertainties in data for the 2-site system were too large for these data to be included. Considering data in the non-Newtonian regime, we see that on a log-log plot ω_z has a linear relationship to $\dot{\gamma}$ which would suggest a power-law $\omega_z = \alpha \dot{\gamma}^\beta$. Coefficients for this relationship are presented in Table 4.4. The coefficient β is seen to decrease with larger molecular weight, *i.e.* at equal strain rates,

the increase of molecular weight results in a decreased propensity for the molecules to rotate. This can be explained by the increased hindrance from surrounding molecules. Note that the systems we consider only approach the entanglement regime for 100-site molecules.

There is again little difference between the results for FENE and FJC molecules. The greatest difference is in the 50-site data where the error bars are much larger for FENE molecules. This would indicate that there is more variation in the angular velocity of FENE molecules than FJC molecules, however, it is unclear whether this is an artifact of the averaging process. If this is not just artifact, it is unclear what the cause is of this variation.

| molecule | α | β ($\omega_z = \alpha \dot{\gamma}^\beta$) |
|---------------|----------|--|
| 4-site FENE | 0.733 | 2.34×10^{-1} |
| 4-site FJC | 0.743 | 2.37×10^{-1} |
| 10-site FENE | 0.648 | 9.96×10^{-2} |
| 20-site FENE | 0.552 | 3.41×10^{-2} |
| 20-site FJC | 0.575 | 3.55×10^{-2} |
| 50-site FENE | 0.311 | 3.75×10^{-3} |
| 50-site FJC | 0.339 | 3.46×10^{-3} |
| 100-site FENE | 0.170 | 2.91×10^{-4} |

Table 4.4: Results for the least-squares fit to ω_z in the power-law region for systems under PCF. The simulation results together with these functions are presented in Fig. 4.17

Algorithm efficiency

It is well known that the calculation of forces is the most computationally expensive part of molecular dynamics simulations [AT87]. For this reason it is useful to compare the efficiency of the FENE and FJC force calculations. Within the force calculation the most intensive part is the calculation of interatomic distances. In our simulations this part of the calculation has been accelerated with the use of both neighbour-list and cell method algorithms. We do not discuss this aspect here, referring the reader to the work of Matin

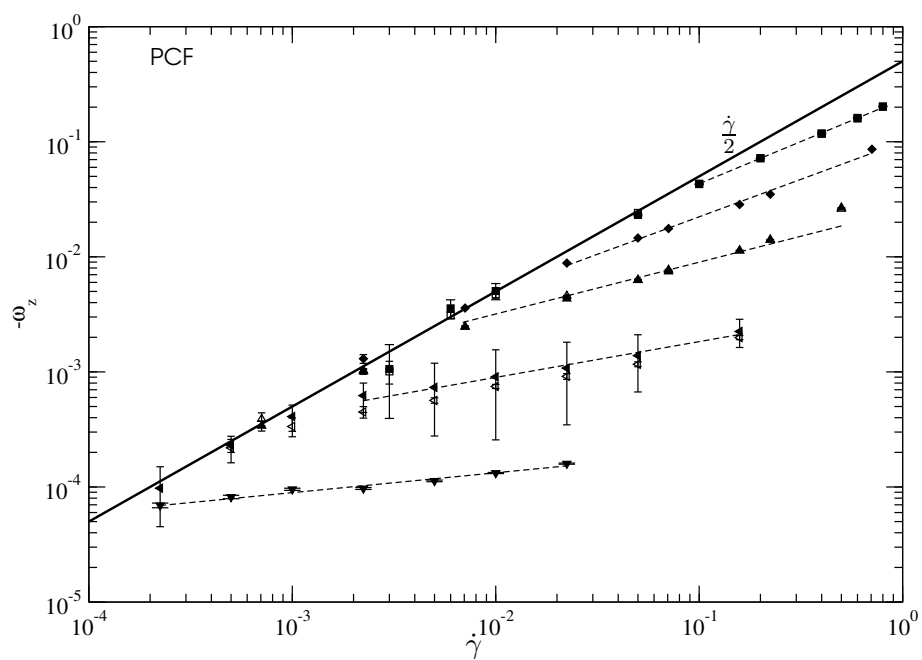


Figure 4.17: The z component ω_z of the average spin angular velocity of molecules for systems under PCF. The line $\omega_z = \dot{\gamma}/2$ has been plotted for comparison in the Newtonian regime. The symbols are the same as in Fig. 4.2. A least-squares fit (dashed lines) to a power law $\omega_z = \alpha \dot{\gamma}^\beta$ is also shown for each molecular weight.

et al. [MDT03]. We have estimated the relative efficiency of the FENE and FJC algorithms and present these details in Table 4.5. These estimates include just the calculation of the forces once the distance between atoms has been determined. It is seen that the FENE calculation represents only a small percentage of the full simulation and does not increase above 5% for the systems studied here. In contrast the constraint calculation for FJC simulations is found to represent an increasing percentage of the simulation time. The efficiency of the constraint algorithm is limited by the linear algebra calculation involved [ME91]. The algorithm uses a *general* LU solver [HJ85] which does not take into account the sparse nature of the constraint matrix. This deficiency has recently been investigated by P.J. Daivis, and we are informed [Tod07] that the efficiency of the constraint algorithm has been significantly improved by using sparse matrix solvers. All simulations were performed on the NEC SX-6 supercomputer which has a vector parallel architecture.

| molecule | N_m | t_{FENE}/t_{total} | t_{FJC}/t_{total} | t_{FJC}/t_{FENE} |
|----------|-------|----------------------|---------------------|--------------------|
| 2-site | 500 | 1.9% | 2.0% | 1.0 |
| 4-site | 500 | 3.2% | 4.9% | 1.6 |
| 10-site | 500 | 3.5% | 32% | 11 |
| 20-site | 500 | 4.0% | 41% | 16 |
| 50-site | 256 | 4.1% | 68% | 43 |
| 100-site | 108 | 4.5% | 86% | 260 |

Table 4.5: Comparison of the efficiency of the FENE and FJC algorithms. The times t_{FENE} and t_{FJC} included just force calculation after the distance between atoms has been determined. The time t_{total} used was the total CPU time of test simulations.

Conclusion

In the preceding section we saw that the structural properties of FENE and FJC molecules were on average almost identical. Given this, we can argue that the rheological properties for the two molecules should also be

very similar in the steady state. Considering that the molecular pressure tensor involves only intermolecular forces and the centre of mass momenta, the contributions to this pressure tensor from the two molecules should be almost the same. In essence any potential between adjacent beads along the chain which give the same structure to a molecule will result in similar rheological properties in the steady state.

It has been shown [EME87] that for identical systems, the atomic pressure tensor gives the same result as the molecular pressure tensor in the steady state. However, the results of these functions under transient flows differ. Again we would expect that the use of the molecular pressure tensor in transient flows will give the same results for FENE and FJC molecules. However, if we used the atomic pressure tensor, we would expect there to be a difference between the molecules since the atomic pressure would include intramolecular forces in the calculation differentiating between FENE and FJC systems.